

## Multiwavelength Spectral Study of 3C 279 in the Internal Shock Scenario

M. Joshi, S. Jorstad, A. Marscher<sup>1</sup>, M. Böttcher<sup>2</sup>, I. Agudo<sup>1&3</sup>, V. Larionov<sup>4</sup>, M. Aller<sup>5</sup>,  
 M. Gurwell<sup>6</sup>, A. Lähteenmäki<sup>7</sup>  
*Boston University, Boston, MA, USA<sup>1</sup>, Ohio University, Athens, OH, USA<sup>2</sup>, IAA, Granada, Spain<sup>3</sup>,  
 St. Petersburg State University, St. Petersburg,  
 Russia<sup>4</sup>, University of Michigan, Ann Arbor, MI,  
 USA<sup>5</sup>, SAO, Cambridge, MA, USA<sup>6</sup>, Metsähovi Radio Observatory, Kylmäla, Finland<sup>7</sup>*

We have observed 3C 279 in a  $\gamma$ -ray flaring state in November 2008. We construct quasi-simultaneous spectral energy distributions (SEDs) of the source for the flaring period of 2008 and during a quiescent period in May 2010. Data have been compiled from observations with Fermi, Swift, RXTE, the VLBA, and various ground-based optical and radio telescopes. The objective is to comprehend the correspondence between the flux and polarization variations observed during these two time periods by carrying out a detailed spectral analyses of 3C 279 in the internal shock scenario, and gain insights into the role of intrinsic parameters and interplay of synchrotron and inverse Compton radiation processes responsible for the two states. As a first step, we have used a multi-slice time-dependent leptonic jet model, in the framework of the internal shock scenario, with radiation feedback to simulate the SED of 3C 279 observed in an optical high state in early 2006. We have used physical jet parameters obtained from the VLBA monitoring to guide our modeling efforts. We briefly discuss the effects of intrinsic parameters and various radiation processes in producing the resultant SED.

### I. INTRODUCTION

Blazars are well known for their variability and power of polarized radiation across a wide range of the electromagnetic spectrum [16, 24, 25]. In some cases, the flux can vary on timescales as short as an hour or less [see e.g., 4, 22]. Blazars exhibit a doubly-peaked spectral energy distribution (SED), in which the low-energy component could extend from radio through UV or X-rays while the high-energy component extends from X-rays to  $\gamma$ -rays. The low-frequency component of the SED is almost certainly due to synchrotron emission from nonthermal, ultra-relativistic electrons. The high-frequency component, on the other hand, is a result of inverse Compton scattering of seed photons by the same ultra-relativistic electrons producing synchrotron emission (in a leptonic jet scenario). In this case, the seed photons could be the synchrotron photons produced within the jet (synchrotron self Compton, SSC) [21, 31], and/or external photons entering the jet from outside (the EC process) [e.g., 8, and references therein]. The spectral variability patterns and SEDs are key ingredients in determining the acceleration of particles and the time-dependent interplay of various radiation mechanisms responsible for the observed emission.

Another defining characteristic of blazars is the high degree of linear polarization at optical wavelengths. Many bright  $\gamma$ -ray blazars that are in the *Fermi-LAT* Bright  $\gamma$ -Ray Source List [2] have shown spectral and linear polarization variability [15, 18, 30]. Linear polarization at mm, IR, and optical wavelengths tends to exhibit similar position angles and sometimes correlation across these wavebands, often with some time delay [15, 19, 20, 25, 28]. Such correspondence between

the variation in polarization and flux across a wide range of the electromagnetic spectrum, combined with VLBI imaging, can be used to identify the location of variable emission at all wavebands and shed light on the physical processes responsible for the variability [30].

The blazar 3C 279, located at a redshift of 0.538 [11], is one of the most prominent and well-studied blazars. This is due to its highly variable nature (change in magnitude  $\Delta m \sim 5$  at optical bands) at all wavelengths and high optical polarization up to 45.5% observed in the U band [32]. Intensive multi-wavelength campaigns [see, e.g., 12, 14, 27] and theoretical efforts [e.g., 7, 10] have led to some important conclusions about the physical properties of 3C 279. Chatterjee et al. (2008) showed that the flux variability in 3C 279 has been found to be significantly correlated at X-rays, optical R band, and 14.5 GHz wave bands, which also suggests that nearly all X-rays are produced in the jet. The X-ray flux has also been associated with superluminal knots, as suggested by correlation with the flux of the core region in the 43 GHz VLBA images [12]. Nevertheless, the nature and origin of its high-energy emission and the relationship of its behavior to the physical aspects of the jet remain elusive [13, 27]. In addition, the correspondence between high- and low-energy emission is also not very well understood.

Here, we aim to understand the physical state of 3C 279 at different flux levels and look for a correspondence between the flux and polarization variation observed during the flaring state of November 2008 and quiescent state of May 2010. This can be achieved by carrying out a detailed spectral analyses of 3C 279 under the internal shock scenario, and understanding the role of intrinsic parameters and interplay of syn-

chrotron and inverse Compton radiation processes in shaping the corresponding spectra of the two states.

As a first step toward comparing the physical state of 3C 279 at different flux levels, we use the multi-slice time-dependent leptonic jet model of Joshi & Böttcher (2011) (in the framework of internal shock scenario) with radiation feedback to simulate the SED of 3C 279 corresponding to the optical high state of early 2006. The broadband emission of 3C 279 for this state indicates suppressed external Compton emission, which makes it an ideal candidate for simulation using a synchrotron-SSC model. We use physical jet parameters obtained from the VLBA monitoring to guide our modeling efforts and discuss the role of various intrinsic parameters and radiation processes in producing the resultant SED.

We briefly describe the model of Joshi & Böttcher (2011) in §II. We discuss our findings about the connection between the flux and polarization variation observed in 3C 279 during flaring and quiescent periods of November 2008 and May 2010, respectively, in §III. We discuss our first results from this study in §III A. We summarize and give a brief description of future work in §IV.

## II. INTERNAL SHOCK MODEL

The mode of acceleration of particles to highly relativistic energies and its location in the jet is not yet completely understood. A colliding shell or an internal shock model offers a way to gain insight into the physics of particle acceleration. Under this model, the central engine (black hole + accretion disk) is assumed to spew out shells of plasma with different velocity, mass, and energy. An inner shell, ejected at a later time, and travelling with a higher speed catches up to a slower moving outer shell that is ejected at an earlier time. The subsequent collision results in an emission region, as shown in Figure 1, with two internal shocks (reverse (RS) and forward (FS)) separated by a contact discontinuity (CD) and traveling in opposite directions to each other in the frame of the shocked fluid. As the shocks propagate through the emission region, they convert the ordered bulk kinetic energy of the plasma into the magnetic field energy and random kinetic energy of the particles. The highly accelerated particles then radiate and produce the emission observed from the jet. The treatment of shell collision and shock propagation is hydrodynamic and relativistic in nature [6, 34].

The model follows the evolution of the electron and photon populations inside the emission region in a time-dependent manner. The equations governing this evolution are,

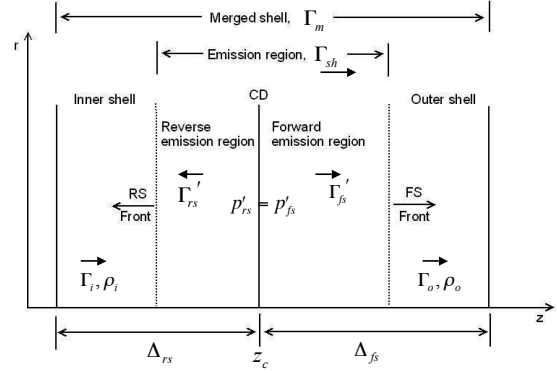


FIG. 1: Schematic of the emission region with RS travelling into the inner shell and FS moving into the outer shell. The bulk Lorentz factors (BLFs) of the two shells are  $\Gamma_i$  &  $\Gamma_o$ , respectively, such that  $\Gamma_i > \Gamma_o$ . The primed quantities refer to the comoving frame and unprimed refer to the lab (AGN) frame. The comoving pressures  $p'_{fs}$  and  $p'_{rs}$  of the shocked fluids across the CD are considered equal.  $\Delta_{rs}$  and  $\Delta_{fs}$  are the widths of the inner and outer shells, respectively, after the collision. The quantities have been obtained by using hydro - dynamic and relativistic jump conditions across the shocks and CD [6, 34].

$$\frac{\partial n_e(\gamma, t)}{\partial t} = -\frac{\partial}{\partial \gamma} \left[ \left( \frac{d\gamma}{dt} \right)_{loss} n_e(\gamma, t) \right] + Q_e(\gamma, t) - \frac{n_e(\gamma, t)}{t_{e,esc}} \quad (1)$$

and

$$\frac{\partial n_{ph}(\epsilon, t)}{\partial t} = \dot{n}_{ph,em}(\epsilon, t) - \dot{n}_{ph,abs}(\epsilon, t) - \frac{n_{ph}(\epsilon, t)}{t_{ph,esc}}. \quad (2)$$

Here,  $(d\gamma/dt)_{loss}$  is the particle (referred to as electrons in the rest of the text) energy loss rate due to synchrotron and inverse Compton losses. The quantity  $Q_e(\gamma, t)$  is the sum of external injection of electrons and intrinsic  $\gamma - \gamma$  pair production rate, and  $t_{e,esc}$  is the electron escape time scale. The quantities  $\dot{n}_{ph,em}(\epsilon, t)$  and  $\dot{n}_{ph,abs}(\epsilon, t)$  are the subsequent photon emission and absorption rates, and  $t_{ph,esc}$  is the photon escape timescale (see §II A). The radiative energy loss rates and photon emissivities are calculated using the time-dependent radiation transfer code of Joshi & Böttcher (2011).

The model reproduces the NIR to  $\gamma$ -ray emission from blazars as it follows the evolution of the emission region out to sub-pc scales only. Thus, it simulates the early phase of  $\gamma$ -ray production. During this time, the radiative cooling is strongly dominant over adiabatic cooling and the emission region is highly optically thick at GHz radio frequencies. Hence, the simulated radio flux is well below that of the actual radio data.

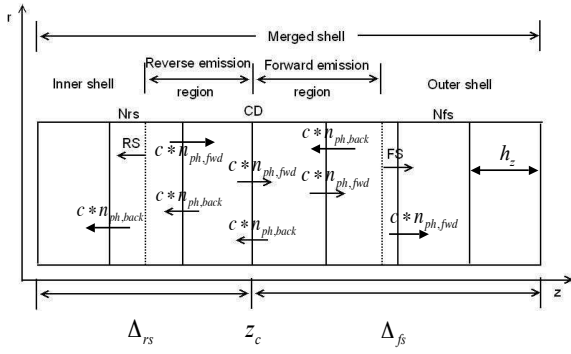


FIG. 2: Schematic of the radiative transfer in between the zones using the appropriate photon escape probability function. The unprimed  $n_{\text{ph}, \sim \text{fwd}/\text{back}}$  values represent the photon densities in the forward and backward direction, respectively, in the comoving frame of the emission region. The rest of the unprimed quantities refer to the lab frame.

### A. Multi-zone Radiation Transfer Method

We calculate the resultant spectrum from the collision, for a cylindrical emission region, in a time-dependent manner. We consider the inhomogeneity in the photon and electron energy density throughout the emission region by dividing the region into multiple zones and providing a fraction of the photon flux from each zone to its adjacent zones in the two directions, as shown in Figure 2.

The fraction of photon flux from a zone or, in other words, the photon escape rate of a zone in a particular direction is calculated using the photon density of that zone and the probability of escape,  $P$ , for a photon from that zone in that direction (forward, backward, or sideways), according to the equation

$$\frac{dn_{\text{ph}, \text{fwd}/\text{back}/\text{side}}(\epsilon, \Omega)}{dt} = \frac{n_{\text{ph}}(\epsilon, \Omega)}{t_{\text{ph}, \text{esc}}} P_{\text{fwd}/\text{back}/\text{side}}, \quad (3)$$

where  $t_{\text{ph}, \text{esc}}$  is the volume-and-angle-averaged photon escape timescale for a cylindrical region that is calculated semi-analytically in the model. We use this framework to calculate the radiation transfer within each zone and in between the zones [26].

## III. THE BLAZAR 3C 279

Analytical studies of the SEDs of 3C 279, collected during the lifetime of CGRO, indicate that the SSC mechanism is responsible for producing X-rays [10, 29]. Intensive multiwavelength campaigns [see e.g. 12, 14, 27] and theoretical efforts [see e.g. 7, 17] have provided insights on the physical properties of 3C 279. But many aspects of the radiation mechanism responsible for high-energy emission still remain unclear. Also, no consistent trends of cross-correlations have been found between optical, X-ray, and  $\gamma$ -rays

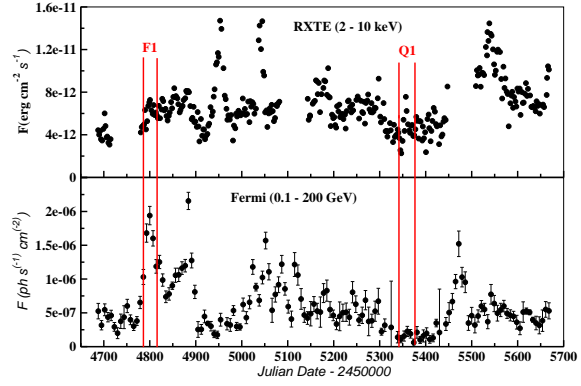


FIG. 3: Observed lightcurves of 3C 279 from 08/09/2008 - 04/16/2011 in  $\gamma$ - and X-ray energy bands. The top panel corresponds to the data compiled from RXTE while the bottom panel refers to the Fermi data. Long-term variability can be seen in the X-rays &  $\gamma$ -rays.

[23] although the source, in early 2009, exhibited coincidence of a  $\gamma$ -ray flare with that in the optical and a dramatic change of optical polarization angle during that time [1]. Such behavior poses a serious challenge to the single-zone leptonic jet model approach where the electron population is assumed to be homogeneous and is responsible for producing synchrotron emission as well as high-energy emission through inverse Compton scattering [13].

In order to improve our insight into the behavior of 3C 279, we aim to understand the evolution of the source at different flux levels by simulating the corresponding SEDs, using a multi-zone leptonic jet model, and looking for connections between the evolution of spectral states and the behavior of the corresponding polarization at optical and radio wavelengths. Figure 3 shows the longterm  $\gamma$ - and X-ray lightcurves (LCs) of 3C 279 from August 2008 till April 2011. From these LCs, we have extracted two 1-month time periods: F1 (11/08/2008 - 12/08/2008) and Q1 (05/22/2010 - 06/26/2010), corresponding to a  $\gamma$ -ray flaring and a quiescent period, as shown in Figures 4 & 5.

As can be seen from Fig. 3, long-term variability exists both in the X-rays &  $\gamma$ -rays. On the other hand, in case of F1 (see Fig. 4, more complicated features exist for such shorter time-periods that need to be considered in detail. While no correlation is apparent between the flux and polarization behavior at optical and radio wavelengths for period F1, the VLBA data on 06/14/2010 (period Q1) resulted in a degree of polarization  $p = 4.7 \pm 0.8\%$  and a radio polarization angle  $EVPA = 78.3 \pm 4.9^\circ$ , which agrees very well with the corresponding values of  $p$  ( $8.6 \pm 0.3\%$ ) and  $EVPA$  ( $75.8 \pm 0.9^\circ$ ) at optical R band. This suggests a common source of origin for the two.

The SEDs of 3C 279 corresponding to states F1 and Q1 are shown in Fig. 6. The data have been compiled from observations with Fermi, Swift, VLBA, and various ground-based optical and radio telescopes.

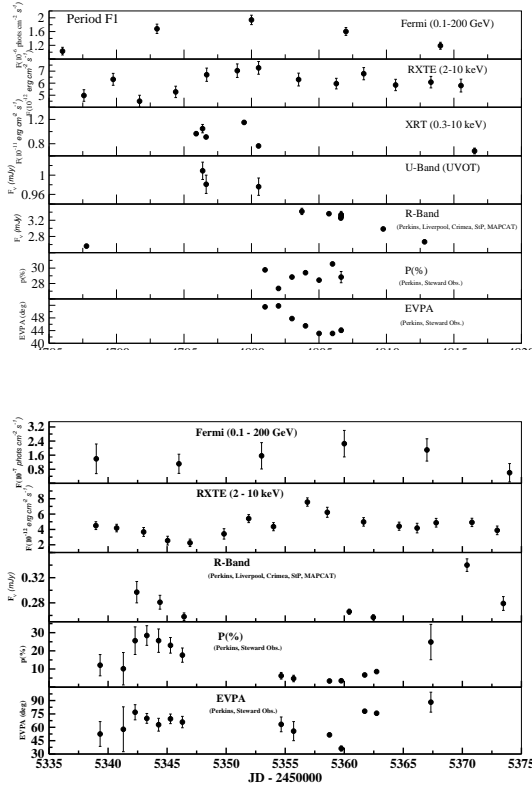


FIG. 5: Multi-frequency lightcurves for the period Q1. R-band fluxes correlate with the optical polarization.

The optical and near-IR data were dereddened using the Galactic extinction coefficients of Schlegel et al. (1998) and the magnitudes were converted to fluxes using the zero-point normalizations of Bessel et al. (1998). The shape of the optical and near-IR spectra indicates that the synchrotron component for both states peaks in the near-IR regime with the  $\nu F_\nu$  value of F1 higher than that of Q1 by almost an order of magnitude. The X-ray flux of F1 remains in a low state coinciding with that of state Q1. The shape of the optical spectrum suggests that the synchrotron component extends into the UV regime with a turnover to the high-energy component taking place at  $\sim 10^{16}$  Hz. The  $\gamma$ -ray spectrum for both states indicates a higher total energy output in the high-energy component compared to the low-energy one, which is typical for the class of flat spectrum radio quasars [8].

### A. First Results

The blazar 3C 279 was observed in an extensive multi-frequency campaign in January 2006 [13]. The object went into an optical flaring state on 01/15/2006. The interesting feature of this state is that the X-ray flux remained in a low state during that period, while coinciding with the historical X-ray low-state of June 2003 [13]. Almost a month later, in February 2006, it was detected by Major Atmospheric Gamma-ray Imaging Cherenkov Telescope (MAGIC) in a very high energy (VHE)  $\gamma$ -ray state [3].

As a first step toward simulating the SEDs of 3C 279

ding

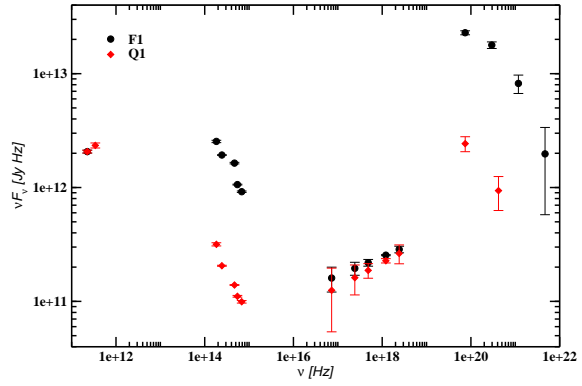


FIG. 6: The observed SEDs of 3C 279 corresponding to periods F1 and Q1.

in order to understand the evolution of spectral states and compare the flaring states of the source in November 2008 and January 2006, we have used the time-dependent leptonic jet model of Joshi & Böttcher (2011) that calculates the synchrotron and SSC radiation to reproduce the observed SED of 3C 279 corresponding to the optical high state of 01/15/2006. Figures 7 & 8 show the instantaneous and time-integrated simulated SEDs of 3C 279, respectively, for this day. The model independent parameters [9] estimated using the SED, VLBA observations [24], and variability on 1-day timescale were used to develop an initial set of input parameters:

$$\begin{aligned}
 \delta &\approx 15.5 \\
 R &\approx 2.5 \times 10^{16} \text{ cm} \\
 B &\approx 0.82 \epsilon_B^{2/7} \text{ G} \\
 \gamma_{\min} &\approx 9.0 \times 10^2 \\
 \gamma_{\max} &\approx 2.2 \times 10^4 \\
 p &\approx 4.3 \\
 \theta_{\text{obs}} &\approx 2.1^\circ \pm 1.1^\circ.
 \end{aligned} \tag{4}$$

Here,  $\delta$  is the Doppler boosting factor. The symbol  $R$  is the radius of the emission region,  $B$  is the comoving magnetic field of the region, and  $\epsilon_B$  is the equipartition parameter between the magnetic field and the electron energy density, assumed to be equal to 1 here. The quantities  $\gamma_{\min}$  &  $\gamma_{\max}$  refer to the low and high energy cutoffs of the electron energy distribution. The spectral index of the electron population, at the time of injection, is given by  $q$  and  $p$  is the equilibrium spectral index obtained using the optical synchrotron spectrum, which is given by  $p = q + 1$  for strongly cooled electrons. The quantity,  $\theta_{\text{obs}}$  is the observing angle inferred from VLBA observations.

The entire emission region has been divided into 100 zones (50 in the forward and 50 in the reverse emission region) to analyze the observed SED of the source. The initial set of parameters was modified to reproduce the state of 3C 279 as observed on 01/15/2006. Various simulations were carried out by varying input parameters one at a time to obtain a reasonable

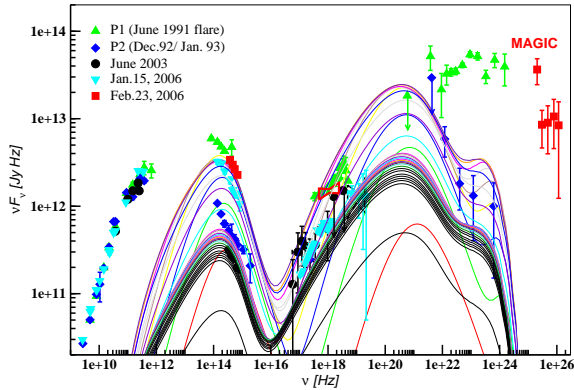


FIG. 7: Simulated instantaneous SEDs of 3C 279 for 01/15/2006 showing the time-dependent evolution of the optical high state. Each solid curve is representative of the spectrum corresponding to a particular instant of time.

fit to the observed SED of 3C 279. A fit is considered successful if it passes through the observed data points, corresponding to 01/15/2006, without over-producing the X-ray flux. An observer’s line of sight angle,  $\theta_{\text{obs}} = 1.6^\circ$ , and a cross-sectional radius,  $R = 6.85 \times 10^{16}$  cm, for the cylindrical emission region, have been chosen to obtain the current best fit. Table I lists the rest of the parameters used for obtaining the current fit of the observed SED. These parameters result in  $\Gamma_{\text{sh}} \approx 18.6$  for the entire emission region,  $B \approx 1.3$  G and  $\gamma_{\text{max}} \approx 1.2 \times 10^5$  for both the forward and reverse emission regions, and  $\gamma_{\text{min, fs}} \approx 1.4 \times 10^3$  &  $\gamma_{\text{min, rs}} \approx 1.7 \times 10^3$  for the forward and reverse emission regions, respectively.

As can be seen from Figures 7 & 8, the observed SED for 01/15/2006 shows a high-energy bump that is indicative of a dominant SSC component and a suppressed EC component. The time-integrated simulated SED of the successful model passes very close to the IR and optical data points, indicating that the synchrotron component is responsible for the lower energy bump of the SED. The spectral upturn takes place in the soft X-rays at  $\geq 0.1$  keV due to the presence of the SSC component in the simulation. The lower-energy part of the SSC component reproduces the X-ray data quite well, suggesting the dominance of the SSC component in producing this part of the high-energy bump. As can be seen in Figure 8, there is a break in the low-energy part of the X-ray spectrum of January 2006 at  $\sim 10^{19}$  Hz, which could be due to the presence of a low-energy cutoff of the electron distribution at ultrarelativistic energies [13].

#### IV. DISCUSSION AND FUTURE WORK

We have presented first results of our study on the behavior of 3C 279 at different spectral states, and the connection between the flaring and quiescent states and the behavior of its polarization at optical and ra-

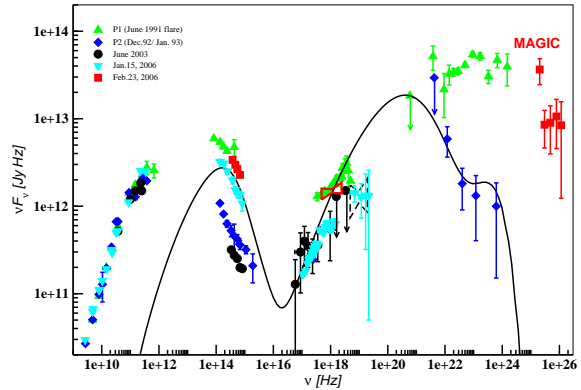


FIG. 8: Simulated time-integrated SED, averaged over 1 day, of 3C 279 for 01/15/2006.

TABLE I: Model parameters used to reproduce the state of 3C 279 as observed on 01/15/2006.

Source	$L_w$	$\Gamma_i$	$\Gamma_o$	$q$	$\epsilon_e$	$\epsilon_B$	$\zeta_e$
	$[10^{48}$ ergs/s]				$[10^{-1}]$	$[10^{-4}]$	$[10^{-2}]$
3C279	1	38	10	4.6	4	5	8

$L_w$ : luminosity of the injected electron population in the blob,  $\Gamma_{i,o}$ : BLFs of the inner and outer shells before collision,  $q$ : particle spectral index,  $\epsilon_e$ : ratio of electron and shock energy density,  $\epsilon_B$ : ratio of magnetic field and shock energy density,  $\zeta_e$ : fraction of accelerated electrons

dio wavelengths.

In order to carry this out, we have extracted a  $\gamma$ -ray flaring (F1) and a quiescent (Q1) state from the long-term LCs of 3C 279 shown in Fig. 3. In case of F1, a clear cross-correlation cannot be seen at optical frequencies over a shorter time-period such as a month (see Fig. 4) and some complicated features exist that need to be considered in detail. In case of Q1, there is an anti-correlation between  $\gamma$ - and X-ray, with X-rays mildly flaring during the  $\gamma$ -ray quiescent state, but the R-band flux shows a strong relationship to the optical polarization (see Fig. 5). On the other hand, while no correlation can be seen between the flux and polarization behavior at optical and radio wavelengths for the period F1, the VLBA data during the Q1 period agrees very well with the corresponding values of  $p$  and  $EVPA$  at optical R band. This suggests a common source of origin for the two during this state.

In order to understand the behavior of the source at different spectral states, it is necessary to simulate the corresponding SEDs of the source. To that end, we have simulated the optical high state of 3C 279 observed in January 2006 using the time-dependent multi-zone leptonic jet model of [26]. The model, in its current form, calculates radiation resulting from synchrotron and SSC processes. The spectral state of 3C 279 observed in January 2006 makes a good candidate for this model, as the  $\gamma$ -ray emission is suppressed in this case and the X-ray emission is generally

associated with SSC scattering [10, 13, 29].

Our current model of the SED results in a high value of  $L_w$  compared with that of Collmar et al. (2010). This is reasonable, as the internal shock model is expected to have low acceleration efficiency, and thus would need a higher kinetic luminosity to achieve the desired acceleration. The current fit results in a value of magnetic field that agrees reasonably well with the model independent parameter estimate and that of Collmar et al. (2010). The value of electron energy index,  $q$ , used to obtain the current fit is almost equal to the model independent parameter  $p$  and is comparatively higher than that of Collmar et al. (2010). This indicates that the synchrotron spectrum in the current fit does not come from a cooled population of electrons. The value of  $q$  needs further adjustment in order to obtain a satisfactory fit. With a successful fit, we hope to gain insights on the acceleration efficiency, the relative speeds with which the two shocks are moving away from each other (in the frame of the shocked fluid), and the mass of each plasma shell needed to reproduce an optical high state of 3C 279 such as that of 01/15/2006.

As part of our future work, the external Compton component due to photons entering the jet from the BLR and dusty torus is being incorporated in the ex-

isting model of [26] to reproduce more fully the SEDs of blazars, especially for flat spectrum radio quasars (Joshi et al. 2012, in prep.), and to analyze a wider variety of blazar spectral states. We plan to use the extended version of the model to simulate the SEDs of 3C 279 for a typical period of 10 days corresponding to F1 and Q1 and compare the results with that of the January 2006 optical high state of 3C 279.

Further, we plan to incorporate the effects of magnetic field orientation, as inferred from polarization monitoring programs, on the resultant spectral variability and SEDs of blazars. This would aid us in the study of intrinsic parameter differences between various blazar subclasses that arise from the orientation of the magnetic field in the jet.

### Acknowledgments

This research was supported in part by NASA through Fermi grants NNX10AO59G, NNX08AV65G, and NNX08AV61G and ADP grant NNX08AJ64G, and by NSF grant AST-0907893.

- 
- [1] Abdo, A. A., et al., 2010, *Nature*, 463, 919
  - [2] Abdo, A. A., et al., 2009, *ApJS*, 183, 46
  - [3] Albert, J., Aliu, E., Anderhub, H., et al., 2008, *Science*, 320, 1752
  - [4] Albert et al., 2007, *ApJ*, 669, 862
  - [5] Bessel, M. S., Castelli, F., & Plez, B. 1998, *A&A*, 337, 231
  - [6] Böttcher, M., & Dermer, C. D., 2010, *ApJ*, 711, 445
  - [7] Böttcher, M., & Principe, D., 2009, *ApJ*, 692, 1374
  - [8] Böttcher, M., 2007, *Ap&SS*, 309, 95
  - [9] Böttcher, M., et al., 2005, *ApJ*, 631, 169
  - [10] Bloom, S. D., & Marscher, A. P., 1996, *ApJ*, 461, 657
  - [11] Burbidge, E. M., & Rosenberg, F. D., 1965, *ApJ*, 142, 1673
  - [12] Chatterjee, Ritaban, et al., 2008, *ApJ*, 689, 79
  - [13] Collmar, W., et al., 2010, *A&A*, 522, 66
  - [14] Collmar, W., Böttcher, M., Krichbaum, T., et al., 2007, *Proc. of 6th INTEGRAL Workshop The Obscured Universe (ESA SP-622)*, eds. S. Grebenev, R. Sunyaev, C. Winkler, p. 207
  - [15] D’Arcangelo, F. D., et al., 2009, *ApJ*, 697, 985
  - [16] D’Arcangelo, F. D., et al., 2007, *ApJL*, 659, 107
  - [17] Dermer, C. D., & Schlickeiser, R., 1993, *ApJ*, 416, 458
  - [18] Gabuzda, D. C., Rastorgueva, E. A., Smith, P. S., & O’Sullivan, S. P., 2006, *MNRAS*, 369, 1596
  - [19] Gabuzda, D. C., Sitko, M. L., & Smith, P. S., 1996, *AJ*, 112, 1877
  - [20] Gabuzda, D. C., & Sitko, M. L., 1994, *AJ*, 107, 884
  - [21] Georganopoulos, M., & Marscher, A. P., 1998, *ApJ*, 506, 621
  - [22] Gaidos, J. A., et al., 1996, *Nature*, 383, 319
  - [23] Hartman, R. C., et al., 2001, *ApJ*, 558, 583
  - [24] Jorstad, S. G., et al., 2005, *AJ*, 130, 1418
  - [25] Jorstad, S. G., et al., 2007, *AJ*, 134, 799
  - [26] Joshi, M., & Böttcher, M., 2011, *ApJ*, 727, 21
  - [27] Larionov, V. M., et al., 2008, *A&A*, 492, 389
  - [28] Lister, M. L., & Smith, P. S., 2000, *ApJ*, 541, 66
  - [29] Maraschi, L., Celotti, A., & Ghisellini, G., 1992, *ApJL*, 397, 5
  - [30] Marscher, A. P., et al., 2010, *ApJL*, 710, 126
  - [31] Marscher, A. P., & Gear, W. K., 1985, *ApJ*, 298, 114
  - [32] Mead, A. R. G., Ballard, K. R., Brand, P. W. J. L., et al., 1990, *A&AS*, 83, 183
  - [33] Schlegel, D. J., Finkbeiner, D. P., & Davis, M. 1998, *ApJ*, 500, 525
  - [34] Spada, M., et al., 2001, *MNRAS*, 325, 1559